



**Faculty of Electrical Engineering and Information
Technology, Slovak University of Technology in
Bratislava**

MUHAMMAD FARAZ UD DIN

Dissertation Thesis Abstract

**Two-dimensional MXenes incorporated Perovskite
Solar Cells**

to obtain the Academic Title of Philosophiae doctor abbreviated
as PhD.

in the doctorate degree study programme: Physical Engineering

in the field of study: Electrical and Electronic Engineering

Form of Study: Full Time

In Bratislava, 2023



Dissertation Thesis has been prepared at
Institute of Physics, Slovak Academy of Sciences, Bratislava, Slovak Republic

Submitter: MUHAMMAD FARAZ UD DIN
Institute of Physics, Slovak Academy of Sciences, Bratislava

Supervisor: RNDr. Eva Majkova DrSc.
Department of Multilayers and Nanostructures, Institute of Physics, Slovak
Academy of Sciences, Bratislava

Readers:

Dissertation Thesis Abstract was sent:

Dissertation Thesis Defence will be held on 4th July 2023 at 9:00 hr

Ing. Stanislav Soja, Ph.D
Prodekan FEI STU



**Fakulta elektrotechniky a informatiky STU v
Bratislave**

MUHAMMAD FARAZ UD DIN

Autoreferát dizertačnej práce

**Perovskitové solárne články so zabudovanými
dvojrozmernými $Ti_3C_2T_x$ MXénmi**

na získanie akademického titulu doktor, v skratke „PhD.

v doktorandskom študijnom programe: fyzikálne inžinierstvo

v študijnom odbore: elektrotechnika

Forma štúdia: denná prezenčná

In Bratislava, 2023

Dizertačná práca bola vypracovaná na

Fyzikálny ústav Slovenskej akadémie vied, Oddelenie multivrstiev a nanoštruktúr

Predkladateľ: MUHAMMAD FARAZ UD DIN

Fyzikálny ústav Slovenskej akadémie vied Oddelenie multivrstiev a nanoštruktúr
Dúbravská cesta 9, Bratislava

Školiteľ: RNDr. Eva Majková, DrSc.

Fyzikálny ústav Slovenskej akadémie vied Oddelenie multivrstiev a nanoštruktúr
Dúbravská cesta 9, Bratislava

Oponenti:

1- Prof. Ing. Július Cirák, PhD.

Pracovisko: Ústav jadrového a fyzikálneho inžinierstva, FEI STU

Adresa pracoviska: Ilkovičova 3, 812 19 Bratislava

2- Dr. rer. nat. Martin Hulman

Pracovisko: Elektrotechnický ústav SAV, v.v.i.

Adresa pracoviska: Dúbravská 9. 841 04 Bratislava

3- Doc. Ing. Miroslav Míkolášek, PhD.

Pracovisko: Ústav elektroniky a fotoniky, FEI STU

Adresa pracoviska: Ilkovičova 3, 812 19 Bratislava

Autoreferát bol rozoslaný:

Obhajoba dizertačnej práce sa bude konať dňa

Ing. Stanislav Soja, Ph.D
Prodekan FEI STU

Contents

Abstract 6

Abstrakt..... 7

Thesis Aim and Objectives 9

Introduction 11

Materials and Methods: 13

Characterization Techniques: 16

Results and Discussions: 16

Conclusions 29

Research Outputs 31

References 33

Abstract

In the past decade, Perovskite solar cells (PSCs) have witnessed remarkable advancements in enhancing power conversion efficiency (PCE), with a significant rise from 3.8% to over 25%. These PSCs consist of multiple layers stack, where the active perovskite layer is positioned between layers that facilitate selective charge transport to the electrodes. The performance of PSCs is dependent on the structure, morphology, and transport properties of these layers and interfaces. To further augment their performance, there is growing interest in exploring the utilization of two-dimensional (2D) nanomaterials, such as MXenes, within PSCs. The incorporation of MXenes offers an exciting prospect to enhance the performance of PSCs.

This work aims to study the PSCs properties with a high-quality NiOx hole transport layer (HTL) prepared by Ion beam sputtering method and to enhance the PCE by utilizing MXene as a dopant in the CH₃NH₃PbI₂ (MAPI) layer. Secondly, investigating the tailoring of electronic properties of MXene mixed ETL was one of the aims to boost the PCE. Finally, the in-situ GIWAXS characterization was applied to investigate the growth of perovskite over the MXene interlayer.

Following the objective of Ph.D thesis, a high-quality 18 nm thick NiOx was prepared by Ion beam sputtering that possesses homogeneous and pinhole-free morphology confirmed by atomic force microscopy (AFM). X-ray diffraction (XRD) revealed a small expansion in the crystalline lattice indicating the presence of a non-stoichiometric NiOx phase. Using NiOx HTLs and MXene-doped MAPI, a 14.3% increase in PCE was observed thanks to a decrease in work function that results in a higher fill factor and open circuit voltage. Secondly, the MXene-mixed SnO₂ electron transport layer (ETL) was applied in n-i-p PSCs, causing the enhancement in PCE from 17.4% to 18.3%. The enhancement is attributed to the improved conductivity of ETL and grain size of perovskite grown over MXene-mixed ETL. The energy-resolved electrochemical impedance spectroscopy (ER-EIS) confirmed the selectivity of MXene doping concentration up to 1 wt.%.

Finally, the growth of the MAPI over MXene interlayer was studied for the system ITO/SnO₂/MXene/MAPI in comparison with that without MXene interlayer by in-situ Grazing Incidence Wide Angle X-ray Scattering measurement. For the perovskite layer grown on the MXene interlayer, an increase of the crystalline domain size of MAPI from 9 nm for SnO₂ layer up to 20 nm for MXene interlayer was observed. Moreover, the MXene interlayer causes a slight increase in the misorientation of the perovskite crystals from $23.2^\circ \pm 1.3^\circ$ to $27.2^\circ \pm 1.6^\circ$ as compared to perovskite growth in the absence of MXene interlayer.

Abstrakt

Perovskitové solárne články zaznamenali významný nárast účinnosti konverzie (PCE) z 3% na 25% v priebehu 10 rokov. Perovskitové solárne články (PSC) sú multivrstvy, kde aktívna perovskitová vrstva je umiestnená medzi vrstvami umožňujúcimi selektívny transport náboja k elektródam. Štruktúra, morfológia a transportné vlastnosti vrstiev a rozhraní určujú funkčnosť PSC. Aplikácia nízkorozmerných (LD) nanomateriálov v našom prípade nanovločiek MXénov v štruktúre PSCs pre zlepšenie ich funkcionality je predmetom aktuálneho záujmu výskumníkov.

Práca je zameraná na štúdium vlastností perovskitových solárnych článkov s NiO_x vrstvou pre transport dier (HTL) pripravenou naprašovaním pomocou iónového zväzku. Ako absorpčná vrstva bol použitý perovskit MAPI $\text{CH}_3\text{NH}_3\text{PbI}_3$ dopovaný MXénmi s cieľom zvýšiť účinnosť konverzie (PCE) solárneho článku. Ďalším cieľom práce je cielene modifikovať elektrické vlastnosti SnO_2 vrstvy s použitím MXénových nanovločiek. Následne sme vyšetrovali rast perovskitovej vrstvy na vrstve MXénov metódou in situ rtg rozptylu pri malom uhle dopadu (GIWAXS).

V súlade s cieľmi práce sme pripravili NiO_x vrstvu pre transport dier (HTL) metódou naprašovania pomocou iónového zväzku na ITO substrátoch. Ako absorpčná vrstva bol použitý perovskit MAPI $\text{CH}_3\text{NH}_3\text{PbI}_3$ dopovaný MXénmi s cieľom zvýšiť účinnosť konverzie (PCE) solárneho článku. Pripravené NiO_x vrstvy hrubé 18 nm boli homogénne, bez dier, čo potvrdila analýza atómovou silovou mikroskopiou. Rtg difrakcia ukázala expanziu kryštalickej mriežky, čo poukazuje na prítomnosť nestechiometrickej NiO_x fázy. Takto pripravené solárne články vykázali účinnosť konverzie zvýšenú o 14,3% v porovnaní s PSC s nedopovaným absorbérom. Toto zvýšenie bolo priradené poklesu výstupnej práce, čo malo za následok vzrast napätia na prázdno a zvýšený faktor plnenia.

Ďalej sme vyvinuli SnO_2 vrstvu pre transport elektrónov v n-i-p PSCs, ktorá zlešila účinnosť PCE zo 17,4 % pre PSC s SnO_2 bez MXénov na 18,3 % pre 0,1 wt% MXénov v ETL. Tento nárast PCE je predovšetkým dôsledkom vyššej vodivosti ETL, čo viedlo aj k vyššej hodnote prúdovej hustoty na krátko ako aj zvýšeniu veľkosti zrn polykryštalickej perovskitovej vrstvy. Energeticky rozlíšena elektrochemická impedančná spektroskopia potvrdila vysokú selektivitu ETL pre obsah MXénov do 1wt%.

Pre perovskitovú vrstvu, ktorá rastla na medzivrstve MXénov bol pozorovaný nárast finálnej kryštalickej domény MAPI z 9 nm pre SnO_2 vrstvu na 20 nm pre MXénovú medzivrstvu.



Rozorientovanosť perovskitových kryštálov v MAPI vrstve mierne vzrástla z $23.2^\circ \pm 1.3^\circ$ na $27.2^\circ \pm 1.6$ pre perovskit, ktorý rástol na MXénovej medzivrstve

Thesis Aim and Objectives

In Perovskite Solar Cells (PSCs), perovskite film morphology and crystalline structure play a crucial role in the performance of PSCs. Despite development made in PSCs, it is challenging to simultaneously control the film morphology and crystalline structure and to prepare high-quality perovskite films with uniform morphology, complete surface coverage and well crystalline grains. The non-compact and poor crystalline perovskite results in poor adhesion, charge traps at the grain boundaries (GBs) of perovskite layer and interfacial recombination with the connecting layers. The noncompact layers create open grain boundaries, which results in charge traps among those GBs, resulting in high trap density. Furthermore, compact perovskite layers have fused GBs resulting in low trap density. Moreover, the size of the grains is also crucial and it reduces the charge recombination by reducing the overall grain boundaries. Similarly, suitable charge-selective layers are also crucial for overall device performance. The ideal charge-selective layers have high mobility, conductivity and perfect band alignment with the perovskite layer; thus, several strategies are required to improve the charge-selective layers as well as the active layer. Two-dimensional nanomaterials additives are therefore considered suitable to improve device performance and stability. In addition, a systematic investigation of how these additives contribute to the morphology and different photophysical processes at the device interfaces is required. Efforts need to be implemented concerning the materials, device architecture, perovskite film morphology and charge-selective layers properties to significantly enhance and stabilize the perovskite solar cells for commercial applications.

Objectives

- 1- Preparation of high quality, homogenous and pinhole-free NiOx layers by Ion beam sputtering method.
- 2- To enhance the power conversion efficiency of inverted perovskite solar cells by utilizing Ti_3C_2 MXenes as a dopant in the active layer.
- 3- To investigate the electron transport layer (ETL) morphological and electronic properties by mixing with MXenes.
- 4- To study the growth of perovskite in high humidity.
- 5- To investigate the perovskite growth over MXene-mixed ETL



- 6- To fabricate efficient n-i-p planar perovskite solar cells using MXene-mixed ETL.
- 7- To study the perovskite growth over the MXene interlayer between ETL and perovskite by In-situ GIWAXS measurements.

Introduction

As a result of the continuous increase in global energy consumption, there is a growing necessity to investigate and develop renewable and sustainable energy sources. This is important to mitigate the negative effects of energy usage on the environment and ensure energy security. Solar energy is widely regarded as the most promising resource to address future energy crises while minimizing adverse impacts on the climate. It offers an efficient and eco-friendly means of converting light energy into electricity. However, for solar technology to be globally established, improvements are needed in terms of devices and materials to enhance power conversion efficiency, stability, and reduce fabrication costs [1]. Recently, perovskite solar cells (PSCs) have been proposed as an environmentally friendly and efficient renewable energy source to tackle future energy challenges without harming the environment [2], [3].

Perovskite solar cells, also known as hybrid perovskite solar cells, have rapidly emerged as a highly promising technology in the field of solar energy conversion. These cells are composed of a material called perovskite, which possesses a unique crystal structure with exceptional electronic properties. These properties include a high absorption coefficient [4], long charge carrier lifetime [5], and low recombination rate [6]. Such characteristics make perovskite solar cells highly effective at converting sunlight into electricity, with recent power conversion efficiencies (PCE) surpassing 25% [7]. This represents a significant improvement compared to traditional solar cell technologies like silicon-based cells.

One of the captivating features of perovskite solar cells is their low-cost production. The materials used in their fabrication are abundant and inexpensive, and the manufacturing process itself is relatively simple. Consequently, perovskite solar cells have the potential to be a cost-effective alternative to traditional solar cell technologies [8], [9].

Despite the remarkable progress achieved in the development of PSCs, there are still several challenges that must be addressed before they can be mass-produced and commercialized. One crucial challenge is ensuring the stability of the cells. PSCs are susceptible to degradation when exposed to moisture and heat, leading to a decline in their performance over time [10],[11]. Therefore, further research is necessary to develop methods that enhance the stability of perovskite solar cells, enabling them to withstand harsh environmental conditions.

In a typical PSC architecture, a perovskite layer is sandwiched between charge-selective layers (HTL and ETL) with electrodes at both ends. The selection of these layers depends on their compatibility with the perovskite absorber layer, including factors such as energy level alignment and conductivity with the active layer [12], [13]. Each of these layers plays a significant role in the overall performance of the device. In recent years, particular attention has been given to improving the quality of the perovskite layer and the properties of the ETL. The grain size of the perovskite materials is a critical factor that impacts the performance of perovskite solar cells. Controlling the grain size can be achieved by adjusting synthesis conditions such as temperature, precursor concentration, and reaction time [14]. However, the presence of defects and impurities often limits the grain size of perovskite materials, hindering the growth of larger grains. Furthermore, improving the electron transport and band alignment of the ETL with the perovskite is crucial for enhancing overall device efficiency. Recently, two-dimensional MXenes have emerged as fascinating materials for improving perovskite quality and ETL properties [15], [16], [17].

MXenes are two-dimensional materials composed of nitrides, carbonitrides, and carbides with varying flake sizes. They are highly conductive due to their metallic nature. The surfaces of MXenes are terminated with functional groups, and their conventional formula is written as $M_{n+1}X_nT_n$, where T represents various functional groups such as OH, F, or O. In this formula, M represents a transition metal, A represents elements from the 13th or 14th group of the periodic table, and X represents carbon and/or nitrogen. The value of n ranges from 1 to 3 [18], [19], [20].

MXenes have garnered considerable attention as promising materials due to their high transmittance, high mobility ($1 \text{ cm}^2 \text{ V}^{-1} \text{ s}^{-1}$), high electronic conductivity ($2 \times 10^4 \text{ S cm}^{-1}$), and high charge carrier density ($3.8 \times 10^{22} \text{ cm}^{-3}$) [21]. Their unique surface termination and rich chemistry provide immense potential for modifying their electronic properties. MXenes have shown great promise in perovskite solar cells. The addition of MXenes can significantly improve the film morphology of the perovskite layer, thereby reducing defect states and charge recombination at the interfaces [15]. Moreover, MXenes can serve as an alternative electron transport layer (ETL) in PSCs by tuning the work function (WF) and enhancing layer mobility. By selecting appropriate transition metals and X elements, MXenes offer the ability to adjust the WF. Additionally, during synthesis, the surfaces of MXenes undergo natural functionalization, altering the electrostatic potential near the surfaces and influencing the electronic structure, resulting in a shift in the WF. In this thesis, MXenes were explored as dopants in the perovskite absorber layer for planar p-i-n

architecture and mixed into the ETL for planar n-i-p architecture PSCs. Various properties were investigated, including perpendicular conductivity, work function (WF), density of states (DOS) measured by energy-resolved electrochemical impedance spectroscopy, ultraviolet photoelectron spectroscopy, and photoluminescence spectroscopy. Structural information was collected using atomic force microscopy (AFM) and scanning electron microscopy (SEM). The results indicate that the use of MXenes as dopants in the active layer enhance grain size and reduces charge recombination. Furthermore, when MXenes are mixed into the ETL, it leads to an enhancement in electrical conductivity. Additionally, the perovskite layer grown over MXene-mixed ETL exhibits a larger grain size compared to the layer grown over unmixed ETL. Furthermore, the perovskite layer annealed in 40% and 60% humidity showed beneficial effects on grain size enhancement, resulting in improved power conversion efficiency (PCE). The grain size of the perovskite layer annealed at 60% humidity with MXene-mixed ETL was particularly enhanced.

Finally, in-situ GIWAXS measurements were conducted on the methylammonium lead iodide (MAPI) layer grown over an MXene interlayer between MAPI and SnO₂ NP, as well as without an interlayer. The size of the crystalline domains in the MAPI layer fabricated over an MXene interlayer remained stable at 20 nm, whereas without the MXene interlayer, it was maintained at 9 nm. Additionally, the MXene interlayer led to a slight increase in the misalignment of perovskite crystals compared to perovskite growth without an MXene interlayer. These attributes highlight the potential of MXenes in perovskite solar cells.

Materials and Methods:

Ion beam sputtering:

IBS, an innovative technique for depositing thin films onto a substrate, involves directing an ion beam toward a target material, resulting in the sputtering and deposition of atoms onto the substrate. This versatile process allows for the deposition of various materials such as metals, semiconductors, and insulators, making it commonly used in the manufacturing of electronic devices like solar cells, thin-film transistors, and optical coatings. Furthermore, ion beam sputtering offers precise and uniform thin film deposition, while also enabling the modification of substrate surface properties.

To create the HTL in a planar p-i-n structure, the NiO_x layer was fabricated using the following method. Initially, the ITO substrates were passed through standard cleaning procedures typically

employed in PSC preparation. Subsequently, the cleaned substrates were placed in an IBS vacuum chamber manufactured by Bestec, Germany, featuring a base pressure of $(1-3) \times 10^{-8}$ mbar. They were then annealed at 120°C for one hour to eliminate any potential contaminants. Additionally, the Ni target was pre-sputtered with pure Ar gas for 20 minutes to eliminate impurities or oxide layers from previous depositions. The actual NiOx sputtering was conducted using a mixture of Ar and O_2 with a flow rate ratio of $\text{Ar}:\text{O}_2 = 5:1$, resulting in a working pressure of 6.4×10^{-4} mbar. The ion source was powered at an RF of 65 W, while the total ion current and accelerating voltage were set at 23 mA and 600 V, respectively. The deposition rate was maintained at $0.08-0.1 \text{ \AA s}^{-1}$, and the process was carried out at room temperature for 30 minutes. Subsequently, the NiOx layers were annealed in air, initially at 250°C for 30 minutes, followed by a final annealing step at 300°C for 5 minutes.

MXenes preparation:

The water-based multilayer MXene paste was acquired from Drexel University located in Philadelphia, USA. By utilizing 1g of the paste, approximately 0.77g of MXene was obtained. At the Polymer Institute, Slovak Academy of Sciences, the delamination reaction was carried out to obtain a few layers MXene flakes. This involved mixing 1g of dried MXene with 1g of LiCl (Sigma Aldrich), followed by stirring the mixture overnight and subsequently centrifuging it multiple times in water at 3500 rpm. To determine the concentration of the resulting product, the few-layer MXenes were filtered using vacuum-assisted filtration to create thin films. Once the MXene films were dried, the concentration was found to be 3 mg/ml.

Preparation of Lead halide perovskite solution:

MAI ($\text{CH}_3\text{NH}_3\text{I}$, 99.5% purity) was acquired from Deysol lmt Sweden, while PbI_2 was purchased from TCI Chemicals. Dimethyl formamide (DMF, 99%) and dimethyl sulfoxide (DMSO, 99.9%) were obtained from Sigma Aldrich. A total of 175 mg of MAI was combined with 507 mg of PbI_2 material. Subsequently, 900 μl of DMF and 100 μl of DMSO were added to the mixture to prepare a perovskite solution with a molar concentration of 1.1 M. The perovskite solution was then stirred overnight at room temperature inside a glovebox.

Planar n-i-p architecture:

The planar n-i-p architecture was used for fabricating the PSCs. The PSCs were created on pre-patterned ITO substrates measuring 19.2×19.0 , which had a sheet resistance of approximately

7 Ω . The substrates underwent a cleaning process involving detergent, acetone, and isopropanol. They were then treated in a UV-Ozone chamber to enhance hydrophilicity and eliminate organic contaminants. Next, a colloidal solution of SnO₂ nanoparticles (80 μ l) was applied to the surface and spun using a spin coater at 3000 rpm for 35 seconds. The SnO₂ nanoparticles layers were annealed at 150 °C for 35 minutes and further treated with UV-ozone for 30 minutes. The resulting SnO₂ nanoparticles layer had a thickness of approximately 30 nm. Following this, the samples were immediately transferred to a glove box for the perovskite spin coating. The perovskite layer was prepared using a two-step method: first, the spin coater was rotated at 1000 rpm for 10 seconds and then at 5000 rpm for 50 seconds. After 5 seconds of the second round, chlorobenzene (CB) (150 μ l) was dropped onto the perovskite layer to initiate crystallization. The perovskite layers were annealed at 50 °C in the dark inside the glove box, followed by annealing at 100 °C at approximately 60% relative humidity. After annealing, the perovskite layers were allowed to cool down in the glove box for 30 minutes before the HTL spin coating process. The perovskite layer had a measured thickness of around 380 nm. Subsequently, a spiro-OMeTAD (HTL) solution (60 μ l) was spin-coated over the perovskite layer at 4000 rpm for 30 seconds. The substrates were then kept in a dry environment for 16 hours before Ag evaporation. The spiro-OMeTAD layer had a thickness of approximately 60 nm. Finally, a layer of Ag (125 nm) was evaporated over the spiro-OMeTAD layer, completing the fabrication of the n-i-p device. The devices were then subjected to J-V and EQE measurements.

Planar Inverted p-i-n architecture:

In the planar inverted p-i-n architecture, the same cleaning process, perovskite spin coating, and Ag evaporation were performed as described for the n-i-p architecture. After the substrate cleaning, a deposition method called Ion beam sputtering was employed to deposit a layer of NiO_x (18 nm) as explained previously. The thickness of the NiO_x layer was measured using a profilometer. Following the NiO_x deposition, perovskite layers were spin-coated onto the substrates and annealed in the glove box at 50 °C in the dark and then at 100 °C. Afterward, a layer of PC₆₁BM was spin-coated at 1020 rpm for 30 seconds, resulting in a thickness of approximately 70 nm. Subsequently, a layer of BCP was spin-coated at 4000 rpm for 30 seconds. Finally, a layer of Ag (125 nm) was evaporated to complete the fabrication of the p-i-n PSCs.

Characterization Techniques:

J-V measurements of the perovskite solar cell: J-V measurements were carried out in a solar simulator (ABET Technologies) under the Air Mass 1.5 Global (AM1.5G) illumination and ambient atmosphere with an intensity of 100 mW.cm^{-2} and a source meter (Model 2400, Keithley Instruments). The solar simulator intensity was calibrated using a standard Si solar cell (Model 91150V, Newport). The external quantum efficiency (EQE) was measured using the SpeQuest system (ReRa Solutions) equipped with a 150 W Xe arc lamp and a monochromator (Omni- λ 300, Zolix).

Ultraviolet photoelectron spectroscopy (UPS): An ultraviolet photoelectron spectroscopy system (UPS, Omicron multi-probe system) with a hemispherical analyzer was used to determine the valence band spectra and Fermi levels. A windowless discharge lamp (Focus HIS13) emitting light in the ultraviolet region (He I, 21.22 eV) was applied for illuminating the sample. For all presented UPS measurements, the energy resolution was less than 100 meV.

Energy resolved-electrochemical impedance spectroscopy (ER-EIS): ER-EIS was employed to investigate the influence of MXene mixing on the electronic density of states (DOS) in the pure and MXene-mixed SnO_2 NP layers. This technique measures the DOS as a function of the energy against vacuum. The details of the method are given elsewhere [22-24].

Photoluminescence: Steady-state photoluminescence (PL) and time-resolved photoluminescence (TRPL) were measured on a PL spectrometer (Edinburgh Instruments, FLS 920) with excitation at 403 nm and a probing laser pulse frequency of 1 MHz. The samples for PL experiments were prepared under the same conditions as for the solar cells, except that the top HTL layer was missing. Instead, the samples were covered by an insulating spin-coated polymer layer of PMMA to protect the perovskite from air during PL measurements.

Results and Discussions:

Following the Ph.D thesis assignments, Figure 1a shows the PSCs that were examined. Figure 1b illustrates the surface topography of the NiOx layer fabricated by ion beam sputtering on an ITO substrate, as observed using AFM. The NiOx layer exhibits a uniform and without pinhole structure, with a surface roughness of 4.2 nm. In Figure 1c, a GIXRD pattern of the NiOx layer is presented, captured at a grazing angle of 0.2° . The pattern reveals three diffraction peaks, which are observed at lower angles compared to the stoichiometric NiO phase possessing a face-centered

cubic (fcc) lattice. This observation suggests a 0.75% expansion of the cubic lattice parameter caused by the excess oxygen, characteristic of the non-stoichiometric NiO_x phase. Furthermore, some ITO diffractions originating from the substrate are visible in the pattern. Figure 1d exhibits the optical transmittances of the bare ITO substrate and the NiO_x layer on ITO. The data clearly indicates that the presence of NiO_x does not significantly affect the optical transmittance in the visible region, as compared to the bare ITO.

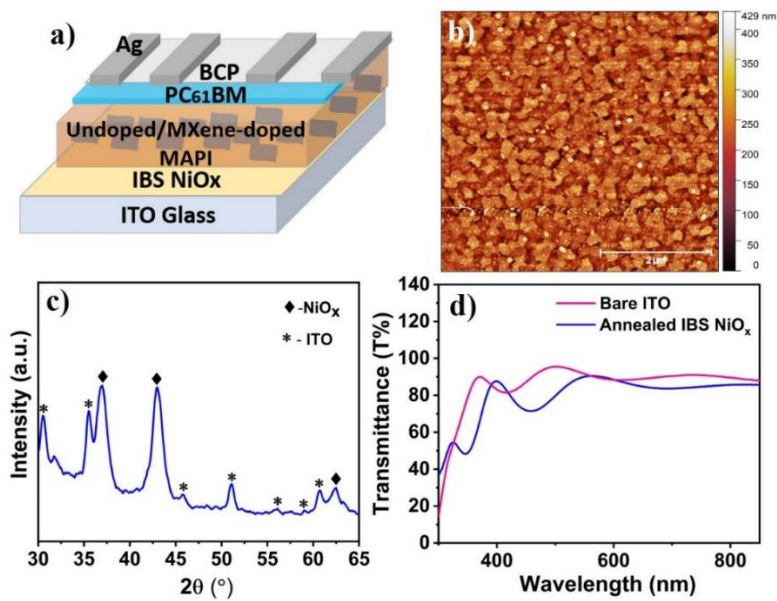


Figure 1. a) PSC design. b) AFM image and c) GIXRD pattern of the NiO_x layer on ITO. d) Transmittance spectra of bare ITO and the NiO_x layer on ITO

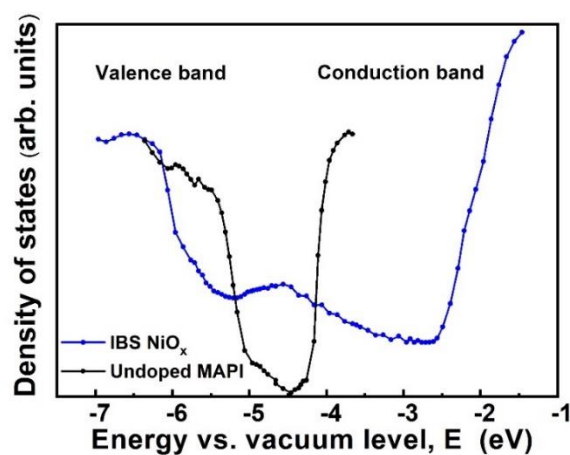


Figure 2. DOS of IBS NiO_x and undoped MAPI layers obtained with ER-EIS.

The DOS evaluation of MAPI and NiOx involved using ER-EIS measurements, as depicted in figure 2. In the conduction band ($E \approx -3.5$ eV), NiOx exhibited a significantly lower DOS, about two orders of magnitude less than that of MAPI. This finding confirms that NiOx functions as an electron-blocking hole transport layer (HTL). Conversely, in the valence band ($E \approx -6$ eV), the DOS of MAPI and NiOx exhibited good alignment, which facilitates the efficient transport of generated holes.

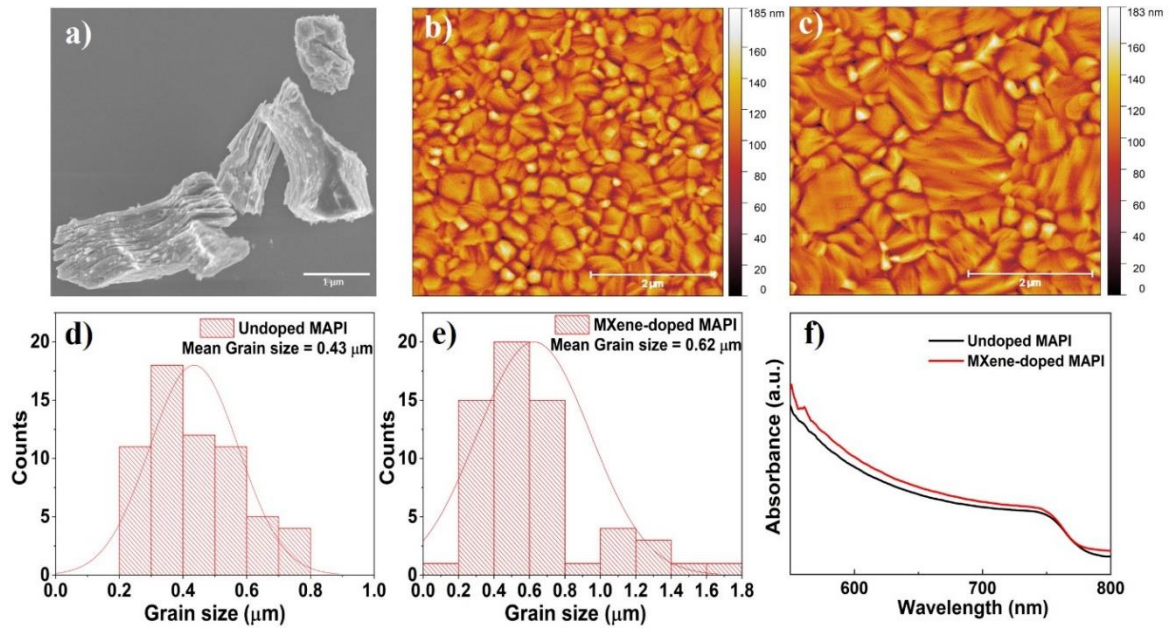


Figure 3. a) Delaminated MXene sheets. AFM images of b) undoped and c) MXene-doped MAPI layers. The grain size distributions of d) undoped and e) MXene-doped MAPI layers calculated from AFM images. f) measured optical absorbance.

In Figure 3a, a scanning electron microscope (SEM) image shows the delaminated multilayer MXene sheets. Figures 3b and 3c present atomic force microscope (AFM) images of MAPI and MAPI layers doped with MXene, respectively. These layers exhibit a uniform spatial distribution and do not have any observable pinholes that could negatively affect their optoelectronic properties. The main advantage of MXene doping is the enlargement of MAPI grain size, resulting in a reduction of the overall grain boundary area. The average grain size of MAPI has increased from 430 ± 80 nm to 620 ± 190 nm due to MXene doping, as shown in the grain size distributions in Figures 3d and 3e, respectively. The larger grain size of MAPI achieved through MXene doping can be attributed to the presence of $Ti_3C_2T_x$ termination groups, which slow down MAPI

crystallization. Furthermore, doping enhances optical absorbance (Figure 3f) by increasing the light absorption by MXene sheets.

The impact of MXene doping on the performance of perovskite solar cells (PSCs) was investigated. PSC devices were prepared using a NiOx layer as the hole transport layer (HTL) and either undoped or MXene-doped methylammonium lead iodide (MAPI) as the photoconversion layer. The best devices showed a 14% power conversion efficiency (PCE) for undoped devices and a 16% PCE for MXene-doped devices, indicating a 14.3% improvement. A 10% average improvement in PCE was observed across 12 devices, consistent with previous studies.

The analysis of current-voltage (J-V) curves and photovoltaic parameters revealed that MXene doping primarily affected the open-circuit voltage (V_{oc}) and fill factor (FF) of the PSCs, rather than the short-circuit current density (J_{sc}) (Figure 4a). This was attributed to the larger grain size and reduced number of grain boundaries in MAPI due to doping, which minimized charge recombination at trap states typically found at grain boundaries. The decrease in non-radiative recombination rate led to an increase in V_{oc} and FF. The EQE measurements showed that MXene doping maintained a nearly wavelength-independent behavior, suggesting that the positive impact of MXene was solely due to improving MAPI crystallization rather than actively participating in charge carrier photogeneration (Figure 4b).

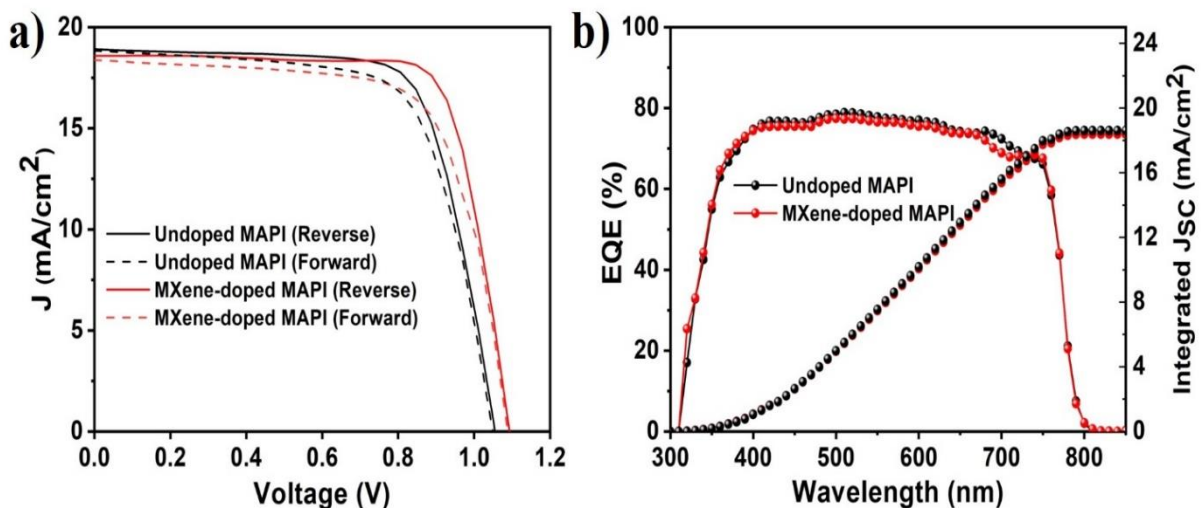


Figure 4. The best undoped and MXene-doped MAPI devices a) J-V curves b) External quantum efficiencies.

Interestingly, despite MXene's high conductivity, it did not result in better J_{sc} . This could be because the large MXene sheets extended to the interfaces between the MAPI layer and the charge extracting layers, creating additional trap states. Moreover, aggregates of MXene sheets on the surface of the MAPI layer were observed, which could act as recombination centers for carriers.

In the second part of Ph.D dissertation, the effect of $Ti_3C_2T_x$ MXene mixed SnO_2 nanoparticles on the electronic properties of ETL was investigated. The concentration range of MXene mixing studied was up to 7.4 wt.%. The effects were analyzed using perpendicular conductivity measurements, density of states (DOS) mapping through energy-resolved electrochemical impedance spectroscopy (ER-EIS), ultraviolet photoelectron spectroscopy (UPS), and photoluminescence. The research confirms that the SnO_2 NP ETL exhibits a hole-blocking behavior for $Ti_3C_2T_x$ MXene concentrations up to 1.0 wt.% as determined by ER-EIS. The highest conductivity is achieved at a concentration of 0.1 wt.% of MXene. At a high MXene concentration of 7.4 wt.%, the MXene's valence band dominates the DOS, peaking at -6.5 eV, suggesting a suppression of the blocking behavior of the MXene-mixed SnO_2 ETL for holes. The study was initiated with the delamination of MXene paste at the Polymer Institute Slovak Academy of Sciences. The delaminated MXenes were analyzed with SEM and STEM. A uniform and dense MXene flakes distributed over the silicon substrate is shown in Figure 5 a and b.

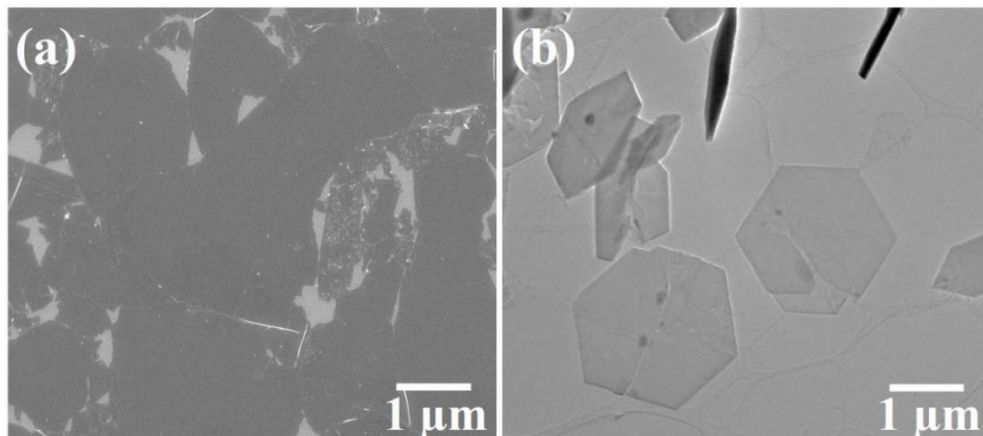


Figure 5. (a) SEM and (b) STEM images of the mono-layer and few-layer MXene nanoflakes. The conductivity of the MXene mixed ETL was investigated using perpendicular geometry with the sample architecture ITO/ SnO_2 -MXene/Ag. The conductivity was calculated using the following equation.

$$I = \sigma_0 A d^{-1} V$$

Where I is the total current, V is voltage, A is the active area (0.015 cm^2) and d is the thickness of the SnO_2 layer (30 nm). The average conductivity values calculated are given in Table 1. An increase in conductivity was observed for all concentrations with a maximum conductivity at 0.1 wt.% MXene.

Table 1. Electrical conductivity values of the MXene-mixed SnO_2 NP layers with different MXene concentrations

| MXene mixing concentration [wt.%] | Conductivity [mS/cm] |
|--------------------------------------|-------------------------|
| 0 | 0.254 ± 0.045 |
| 0.075 | 0.390 ± 0.062 |
| 0.1 | 0.408 ± 0.092 |
| 0.15 | 0.280 ± 0.074 |
| 0.2 | 0.262 ± 0.049 |
| 0.4 | 0.320 ± 0.058 |
| 0.6 | 0.383 ± 0.050 |
| 0.8 | 0.344 ± 0.072 |
| 1 | 0.373 ± 0.084 |

The GIXRD diffraction patterns show SnO_2 regular tetragonal phase after mixing and illustrate not visibly affected by the presence of MXenes. Moreover, ultraviolet photoelectron spectroscopy (UPS) and UV absorption measurements were conducted for the MXene-mixed SnO_2 layers. All the MXene mixing concentrations up to 1 wt.% show a negligible difference in the bandgap and shows low absorption as required for the ETL performance.

The ER-EIS technique was employed to examine the effect of MXene mixing on the density of states (DOS) in the SnO₂ NP layer. In the energy range covered by the ER-EIS technique, the valence band edge of the pristine SnO₂ NP layer, which is expected to be located at -8.4 eV below the vacuum level, is not observable. Conversely, the valence band edge of the pure MXene layer can be detected at -6.0 eV (refer to Fig. 6).

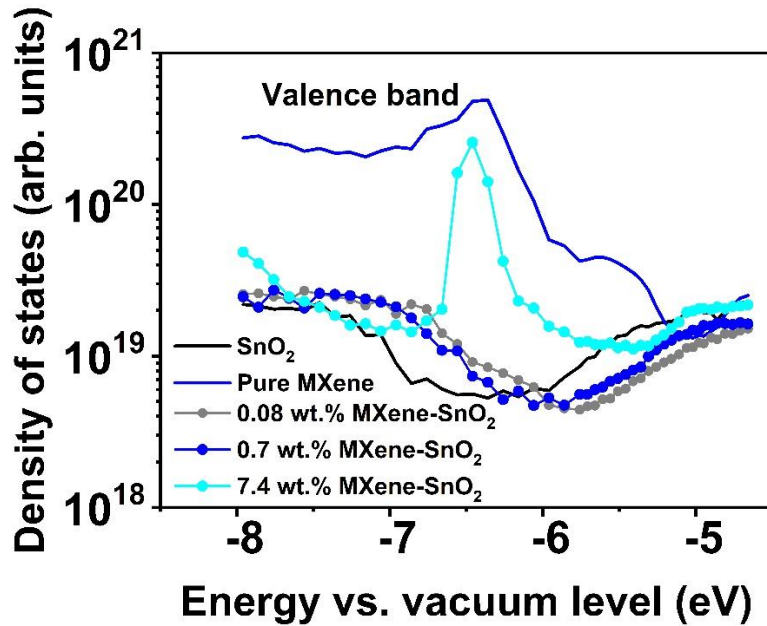


Figure 6. The DOS of the valence band of the pure MXene layer and the SnO₂ NP layers mixed with 0 wt.%, 0.08 wt.%, 0.7 wt.% and 7.4 wt.% MXene on ITO substrates obtained by the ER-EIS.

In order to assess the limitations of incorporating MXene into the SnO₂ to enhance the performance of the electron transport layer (ETL), we conducted experiments involving the deposition of MAPI layers on ITO substrates. These substrates were coated with PEDOT:PSS and SnO₂ NP layers containing different weight percentages (0%, 0.7%, and 7.4%) of MXene. The measurements were carried out using ER-EIS (Fig. 6).

For an accurate ER-EIS measurement of the valence band in a MAPI layer, which is exclusively probed by holes, there needs to be unimpeded hole transport from the MAPI layer across its interface with the underlying layer. As depicted in Fig. 6, the SnO₂ NP layer mixed with 7.4 wt.% MXene exhibits a valence band maximum that is 1.5-2 orders of magnitude higher at -6.5 eV compared to the other layers. This suggests that effective hole transport is facilitated by the valence band in this heavily MXene-mixed SnO₂ NP layer. However, the density of states (DOS) curve of

MAPI on this layer, as shown in Fig. 7, closely resembles that of MAPI on the well-known hole transport PEDOT:PSS layer. Consequently, the heavily MXene-mixed SnO₂ NP layer is deemed unsuitable as an ETL.

On the contrary, both the pure SnO₂ NP layer and the one mixed with 0.7 wt.% MXene exhibit a lack of adequately high DOS for hole transport around -6.5 eV (Fig. 6). As a result, these layers act as barriers for holes, leading to distorted valence band curves of MAPI measured by the ER-EIS (Fig. 7).

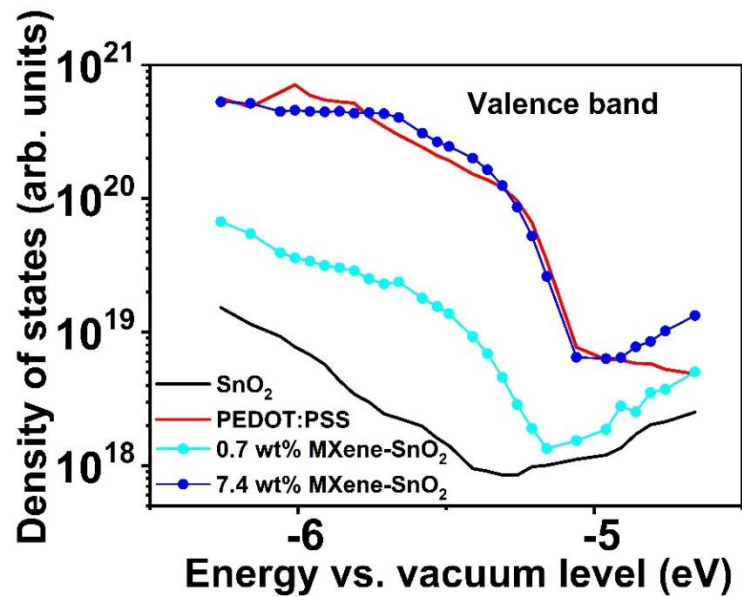


Figure 7. The DOS of the valence band of MAPI layers on the PEDOT:PSS and SnO₂ NP layers with 0 wt.%, 0.7 wt.% and 7.4 wt.% MXene on ITO substrates obtained by the ER-EIS.

The steady-state PL spectra of the ITO/SnO₂ NP/MAPI/PMMA and ITO/0.1wt.% MXene-mixed SnO₂ NP/MAPI/PMMA samples with MAPI layer annealed at 40% and 60% RH show that the PL peak intensity is lower for the 0.1 wt.% MXene-mixed SnO₂ NP ETL at both values of RH suggesting that the electron transfer from the perovskite to the ETL is more efficient and carrier recombination is suppressed when incorporating MXene into the SnO₂ NP ETL.

We have addressed the humidity problem associated with the MAPI perovskite layers that were deposited on SnO₂ NP layers containing 0 and 0.1 wt.% MXene. The deposition of MAPI layers was carried out inside a glovebox, followed by annealing at approximately 40% and 60% relative humidity (RH) using a humidity chamber.

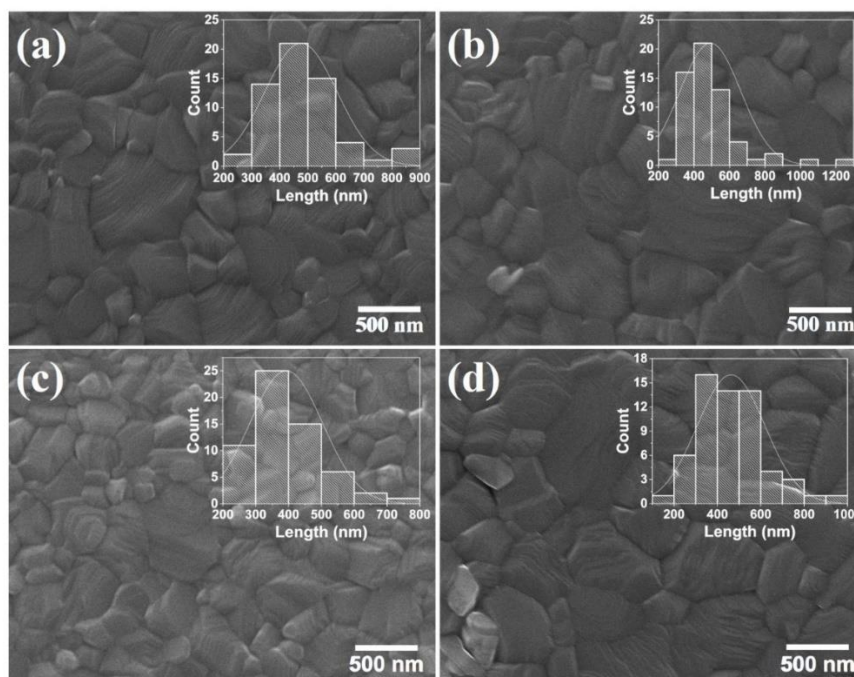


Figure 8. SEM images of the MAPI layer on the (a) 0 wt.% and (b) 0.1 wt.% MXene-mixed SnO₂ NP layer annealed at ~60% RH and the (c) 0 wt.% and (d) 0.1 wt.% MXene-mixed SnO₂ NP layer annealed at ~40% RH. The insets show the grain size distribution of the respective SEM images.

Table 2. The average grain size of MAPI layers on the SnO₂ NP ETLs mixed with 0 and 0.1 wt.% MXene and annealed at ~40% and ~60% RH.

| ETL | grain size at ~40% RH [nm] | grain size at ~60% RH [nm] |
|-----------------------------------|-------------------------------|-------------------------------|
| SnO ₂ | 393 | 475 |
| SnO ₂ + 0.1 wt.% MXene | 463 | 492 |

When examining SEM images (Figs, 8a,c), we observed that for the pure SnO₂ NP layer, the average grain size of MAPI was 393 nm and 475 nm after annealing at approximately 40% RH and 60% RH, respectively. The addition of 0.1 wt.% MXene to the SnO₂ NP layer resulted in further enlargement of the MAPI grain size. Specifically, during annealing at approximately 60%

RH, the average MAPI grain size increased to 492 nm compared to 475 nm on the pure SnO₂ NP layer (Figs. 8a,b, Table 2). The effect of MXene mixing was even more significant during annealing at approximately 40% RH, where the average MAPI grain size increased from 393 nm on the pure SnO₂ NP layer to 463 nm on the SnO₂ NP layer mixed with 0.1 wt.% MXene (Figs 8c,d, Table 2).

These results show that both humidity as well as MXene incorporation into ETL promote the crystallization and grain growth in the MAPI perovskite layer with a beneficial effect on the PCE of the respective device

The SnO₂ NP layer mixed with 0.1 wt.% MXene, which showed the highest conductivity, was chosen to fabricate the ITO/SnO₂-MXene/MAPI/Spiro-OMeTAD/Ag solar cells. The J-V curves of the devices with the pure and 0.1 wt.% MXene-mixed SnO₂ NP ETLs and MAPI annealed at ~40% RH and ~60% RH are shown in Fig 9a. The EQE spectra of the devices with the pure and 0.1 wt.% MXene- mixed SnO₂ NP ETLs and MAPI annealed at ~60% RH are shown in Fig 10. The incorporation of MXenes results in an almost uniform increase of EQE amplitude in the entire spectrum ranging from 350 nm to 700 nm. It is in line with the fact that MXene mixing caused just increasing the size of perovskite grains. The modulation of EQE spectra is caused by the reflectance of the solar cell surface.

Table 3. The best PCE of the devices with the SnO₂ NP ETLs mixed with 0 wt.% and 0.1 wt.% MXene and the MAPI layer annealed at ~40% and ~60% RH.

| MXene concentration | PCE at ~40% RH [%] | PCE at ~60% RH [%] |
|---------------------|-----------------------|-----------------------|
| 0 wt. % | 16.6 | 17.4 |
| 0.1 wt. % | 17.2 | 18.3 |

The best PCE increased from 16.6% to 17.2% and from 17.40% to 18.3% after the 0.1 wt.% MXene mixing for the ~40% and ~60% RH annealing, respectively (Table 3). This PCE increase is related mainly to the increase in J_{sc} , which can be explained by the improved quality of grain boundaries in the MAPI layer annealed at 60% RH, generating fewer defect states in the band gap, as well as by better connectivity between them.

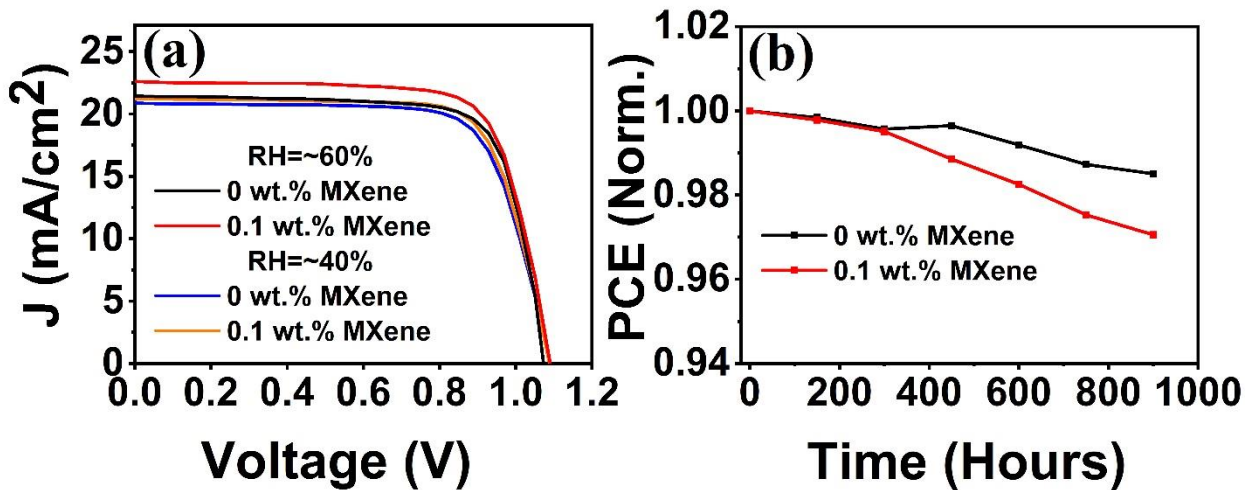


Figure 9. (a) J-V curves of the devices with the 0 wt.% and 0.1 wt.% MXene-mixed SnO₂ NP ETLs and MAPI annealed at ~40% RH and ~60% RH; (b) Temporal evolution of PCE of the devices with the 0 wt.% and 0.1 wt.% MXene-mixed SnO₂ NP ETLs and MAPI annealed at ~60% RH.

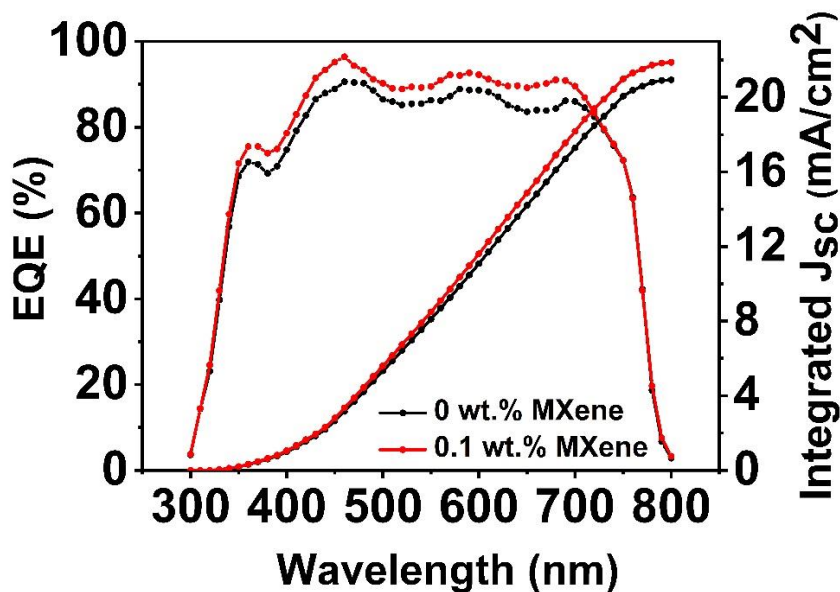


Figure 10. EQE spectra of the devices with the 0 wt.% and 0.1 wt.% MXene-mixed SnO₂ NP ETLs and MAPI annealed at ~60% RH.

To check the stability of the devices, their PCE was tested every 150 hours. The ~60% RH annealed devices with the pure and 0.1 wt.% MXene-mixed SnO₂ NP ETLs retained 98.5% and 97 % of PCE, respectively, after 900 hours of storage in a glove box (Fig. 9b). Considering the sensitivity of MXene to humidity and oxygen, such high stability qualifies the MXene-mixed SnO₂ NP layer as a viable option for the ETL in future commercial perovskite solar cells.

In the final part of Ph.D. dissertation, perovskite crystallization was analyzed over the MXene interlayer using in-situ GIWAXS measurement. In the study, we conducted in-situ grazing-incidence wide-angle X-ray scattering (GIWAXS) measurements using a tabletop laboratory set-up. Then used a microfocus X-ray source with Montel optics to generate X-ray photons with an energy corresponding to CuK α radiation. The photon flux of the X-ray source was 3×10^8 photons/s, and the X-ray beam had a divergence of 5 mrad. The X-ray source was positioned on a hexapod, which adjusted the angle of incidence to 4°. The sample, placed on a hotplate within a plastic box, was subjected to controlled water evaporation to maintain a humidity level of 60% at a temperature of 60 °C. The X-ray measurements were carried out with a sample-detector distance of 103 mm. To capture the GIWAXS maps, a 2D X-ray detector with a pixel size of 172 μm and a resolution of 487 pixels horizontally and 407 pixels vertically was employed. The exposure time for each measurement was set to 1 second.

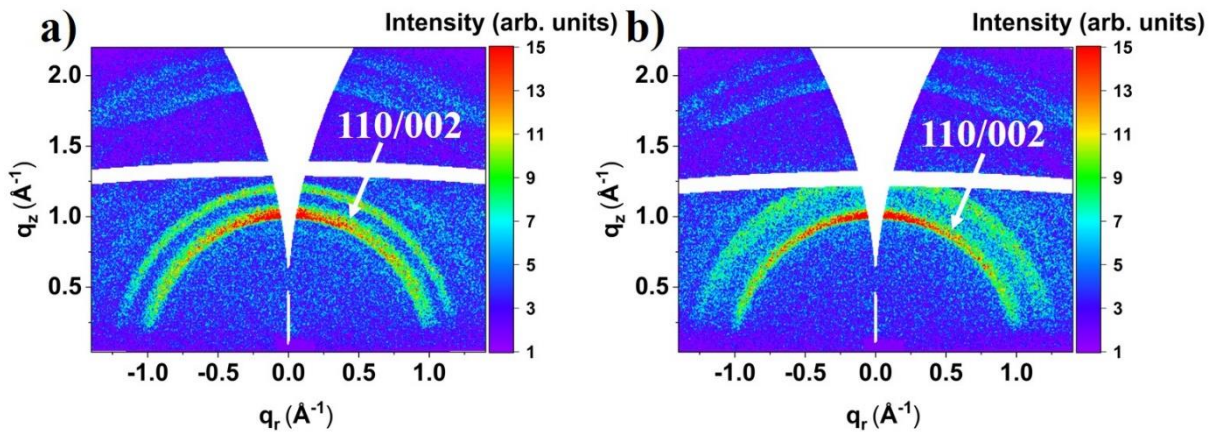


Figure 11. The GIWAXS map of the perovskite layer at the end of thermal annealing for perovskite prepared on the standard substrate a) without MXenes and b) with MXenes.

Comparing the GIWAXS maps at the end of thermal annealing for the perovskite layer prepared on the standard substrate without MXenes and modified with MXenes is plotted in Fig. 11. We observe 110/002 diffraction ring with some intensity enhancement around q_z axis. This enhancement means that some preferential orientation of perovskite crystals is present around

normal to the sample surface. The quantification of the preferential orientation in perovskite layers is discussed in the text below using the concept of χ angle and χ cuts.

Comparing the 110/002 diffraction peaks for perovskite prepared on the standard ITO-SnO substrate without MXenes and with MXenes at the end of thermal annealing is plotted in Fig. 12.

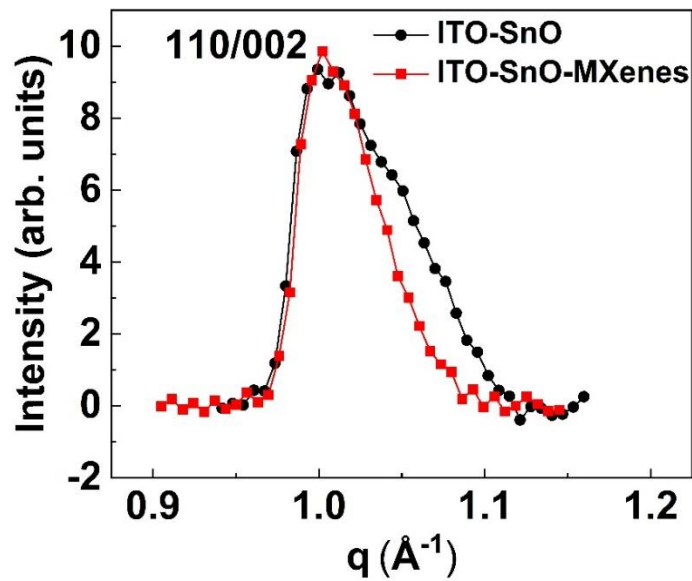


Figure 12. The 110/002 diffraction peak at the end of thermal annealing for perovskite deposited on the standard substrate a) without MXenes (black dots) and b) with MXenes (red squares).

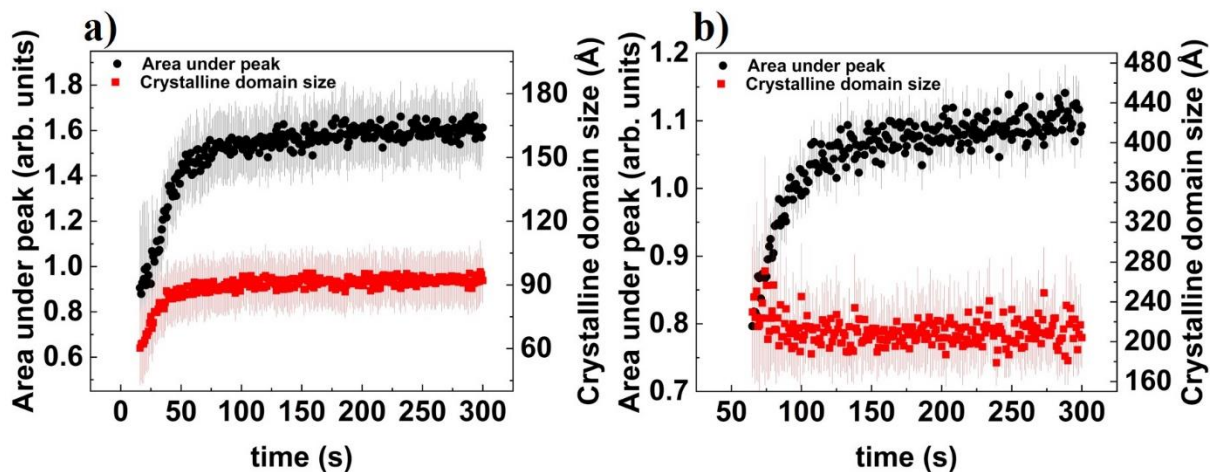


Figure 13. The temporal evolution of area under diffraction peak (black dots) and the crystalline domain size (red squares) for perovskite deposited on the standard substrate a) without MXenes and b) with MXenes.

Fig. 12 clearly shows the narrowing of the 110/002 diffraction peak of perovskite prepared on the substrate modified with MXenes, which suggests larger perovskite crystalline domains for that case.

The evolution of the area under peak and crystalline domain size during thermal annealing for perovskite prepared on the ITO-SnO substrate without MXenes and ITO-SnO substrate with MXenes is plotted in Fig.13. The crystalline domain size of perovskite prepared on the standard substrate without MXenes was stabilized at the value of the 9 nm, while for the substrate with MXenes, it was stabilized at the value of 20 nm. It suggests the growth of the larger crystalline grains on the substrate modified by MXenes.

Conclusions

This thesis focused on investigating the effects of introducing high-quality NiOx HTL layers produced through the IBS technique and MAPI perovskite layers doped with $Ti_3C_2T_x$ MXene on the performance of PSCs. The inclusion of MXene sheets improved the crystallization of the perovskite, resulting in larger grains and fewer grain boundaries, which reduced non-radiative recombination. However, the doping process also introduced defects in the MAPI band gap, offsetting the benefits of larger grains. The enhancements in V_{OC} and FF were attributed to a decrease in the work function of MAPI. The research demonstrated a 14.3% improvement in PCE for PSCs containing 0.15 wt% MXene-doped MAPI layers, with an average improvement of 10%. Furthermore, partially delaminated multilayer MXene sheets showed promise, indicating potential cost and time savings for scaling up production. These findings have important implications for enhancing the performance of inverted PSCs with p-i-n architecture by utilizing high-quality IBS-deposited HTLs and MXene doping of the perovskite layer.

The study also investigated the impact of incorporating $Ti_3C_2T_x$ MXene in different concentrations (0-7.4 wt%) into SnO₂ NP ETL on its electronic properties. Mixing up to 1.0 wt% MXene improved the conductivity of SnO₂ NP ETL, with the highest conductivity observed at 0.1 wt% MXene mixing. The optical bandgap slightly increased with higher MXene concentrations, but the LUMO and HOMO energies remained largely unchanged. ER-EIS confirmed the ETL selectivity of SnO₂ NP with up to 1.0 wt% MXene mixing. However, at 7.4 wt% MXene mixing, the MXene's valence band dominated the DOS, indicating a hindrance in hole blocking by SnO₂ NP. The performance of the SnO₂-0.1wt% MXene mixed ETL was superior to pristine SnO₂ NP ETL, as

observed through PL and TRPL data, resulting in improved PCE (from 16.6% to 17.2%) due to enhanced charge transfer and MAPI crystallization, leading to larger grain size and reduced non-radiative recombination. Annealing the MAPI layer at ~60% RH further improved PCE to 17.4% for pure ETL and 18.3% for MXene mixed ETL. Long-term stability tests showed excellent retention of PCE, with 98.5% and 97% maintained after 900 hours in a glove box for pure and MXene mixed ETLs, respectively. Overall, these findings demonstrate that incorporating MXene into SnO₂ NP ETL holds promise for enhancing the performance of n-i-p perovskite solar cells based on MAPI.

In-situ GIWAXS measurements were conducted to compare the growth of MAPI with and without an MXene interlayer between MAPI and SnO₂ NP. The inclusion of an MXene interlayer maintained the crystalline domains in the MAPI layer at 20 nm, while without the interlayer, it stabilized at 9 nm. The MXene interlayer also caused a slight increase in the misalignment of perovskite crystals compared to growth without the interlayer. These findings highlight the potential of MXenes in improving the performance of perovskite solar cells.

Research Outputs

1- **Muhammad Faraz Ud Din**, Vladimir Held, Sami Ullah, Shima Sousani, Maria Omastova, Vojtech Nadazdy, Ashin Shaji, Peter Siffalovic, Matej Jergel, Eva Majkova, A synergistic effect of the ion beam sputtered NiO x hole transport layer and MXene doping on inverted perovskite solar cells, *Nanotechnology*. 33 (2022) 425202. **(IF: 3.95)**

2- **Muhammad Faraz Ud Din**, Shima Sousani, Mario Kotlar, Sami Ullah, Maros Gregor, Tomas Scepka, Yaryna Soyka, Anastasiia Stepura, Ashin Shaji, Femi Igbari, Vojtech Nadazdy, Peter Siffalovic, Matej Jergel, Maria Omastova, Eva Majkova, Tailoring the electronic properties of the SnO₂ nanoparticle layer for n-i-p perovskite solar cells by Ti₃C₂T_x MXene. Under Review in *Materials Communication Today* **(IF: 3.71)**

3- Sami Ullah*, **Muhammad Faraz Ud Din***, Jafar Khan Kasi, Ajab Khan Kasi, Karo Vegso, Mario Kotlar, Matej Micusik, Mate Jergel, Vojtech Nadazdy, Peter Siffalovic, Eva Majkova, Azhar Fakharuddin, Mesoporous SnO₂ Nanoparticle-Based Electron Transport Layer for Perovskite Solar Cells, *ACS Appl. Nano Mater.* 5 (2022) 7822–7830. ***Authors contributed equally, (IF: 6.14)**

4- Femi Igbari, Fa-Feng Xu, Jiang-Yang Shao, **Muhammad Faraz Ud Din**, Peter Siffalovic, Yu-Wu Zhong, Stacking Interactions and Photovoltaic Performance of Cs₂AgBiBr₆ Perovskite, *Sol. RRL*. 2200932 (2023) 1–28. **(IF: 9.17)**

5- Israt Ali, **Muhammad Faraz Ud Din**, Zhi-Gang Gu, MXenes Thin Films: From Fabrication to Their Applications, *Molecules*. 27 (2022) 1–38. **(IF: 4.92)**

6- Israt Ali, **Muhammad Faraz Ud Din**, Daniele T. Cuzzupè, Azhar Fakharuddin, Hitler Louis, Ghulam Nabi, Zhi-Gang Gu, Ti₃C₂T_x-Modified PEDOT:PSS Hole-Transport Layer for Inverted Perovskite Solar Cells, *Molecules*. 27 (2022). **(IF: 4.92)**

7- Muhammad Adeel Ashraf, Karol Vegso, Ashin Shaji, Michal Bodik, Mayela Garcia Sánchez, Muhammad Zubair, **Muhammad Faraz Ud Din**, Eva Majkova, Andrea Strakova Fedorková, Jozef Keckes, Peter Siffalovic, Aligned Bilayer of Single-Walled Carbon Nanotubes Suppresses the Polysulfide Shuttle in Li-S Batteries, *ACS Appl. Energy Mater.* 5 (2022) 15649–15655. **(IF: 6.95)**

8- Saima Zafar, Muhmmad Zubair, Syed Mujtaba Shah, Muhammad Imtiaz Khan, Abbas Ahmad Khan, Muhammad Faisal Iqbal, Ali Hassan, **Muhammad Faraz Ud Din**, Effect of Fe doping on the structural and optical properties of ZnS macro-spheres, *Optik (Stuttg)*. 262 (2022) 169342. **(IF: 2.84)**

9- Israt Ali, **Muhammad Faraz Ud Din**, Anna Kálosi, Adriana Annušová, Martina Labudová, Yaryna Soyka, Maria Omastová, Matej Jergel, Peter Šiffalovič, Eva Majková, Facile Fabrication of Ti_3C_2 Mxene Nanosheets and Their Photothermal Properties, *NANOCON Conf. Proc. - Int. Conf. Nanomater.* (2021)

10- The effect of $Ti_3C_2T_x$ MXene doping on the electronic properties of SnO_2 nanoparticles films for perovskite solar cells, **Muhammad Faraz Ud Din**, Israt Ali, Vojtech Nádaždy, Matej Jergel, Peter Šiffalovič, Eva Majkova, Anastasiia Stepura, Michal Procházka, Mária Omastová, Poster presentation at 13th Nanocon conference, Brno, Czech Republic (2021)

References

- [1] R. Wang, M. Mujahid, Y. Duan, Z.K. Wang, J. Xue, Y. Yang, A Review of Perovskites Solar Cell Stability, *Adv. Funct. Mater.* 29 (2019) 1–25. <https://doi.org/10.1002/adfm.201808843>.
- [2] T. Wu, Z. Qin, Y. Wang, Y. Wu, W. Chen, S. Zhang, M. Cai, S. Dai, J. Zhang, J. Liu, Z. Zhou, X. Liu, H. Segawa, H. Tan, Q. Tang, J. Fang, Y. Li, L. Ding, Z. Ning, Y. Qi, Y. Zhang, L. Han, The Main Progress of Perovskite Solar Cells in 2020–2021, *Nano-Micro Lett.* 13 (2021). <https://doi.org/10.1007/s40820-021-00672-w>.
- [3] T. Wu, X. Liu, X. Luo, X. Lin, D. Cui, Y. Wang, H. Segawa, Y. Zhang, L. Han, Lead-free tin perovskite solar cells, *Joule.* 5 (2021) 863–886. <https://doi.org/10.1016/j.joule.2021.03.001>.
- [4] N. Ali, N. Shehzad, S. Uddin, R. Ahmed, M. Jabeen, A. Kalam, A.G. Al-Sehemi, H. Alrobei, M.B. Kanoun, A. Khesro, S. Goumri-Said, A review on perovskite materials with solar cell prospective, *Int. J. Energy Res.* 45 (2021) 19729–19745. <https://doi.org/10.1002/er.7067>.
- [5] J. Luo, W. Zhang, H. Yang, Q. Fan, F. Xiong, S. Liu, D. Li, B. Liu, Halide perovskite composites for photocatalysis: A mini review, *EcoMat.* 3 (2021) 1–16. <https://doi.org/10.1002/eom2.12079>.
- [6] A.E. Shalan, E. Akman, F. Sadegh, S. Akin, Efficient and Stable Perovskite Solar Cells Enabled by Dicarboxylic Acid-Supported Perovskite Crystallization, *J. Phys. Chem. Lett.* 12 (2021) 997–1004. <https://doi.org/10.1021/acs.jpcllett.0c03566>.
- [7] H. Min, D.Y. Lee, J. Kim, G. Kim, K.S. Lee, J. Kim, M.J. Paik, Y.K. Kim, K.S. Kim, M.G. Kim, T.J. Shin, S. Il Seok, Perovskite solar cells with atomically coherent interlayers on SnO₂ electrodes, *Nature.* 598 (2021) 444–450. <https://doi.org/10.1038/s41586-021-03964-8>.
- [8] C. Wu, K. Wang, Y. Jiang, D. Yang, Y. Hou, T. Ye, C.S. Han, B. Chi, L. Zhao, S. Wang, W. Deng, S. Priya, All Electro Spray Printing of Carbon-Based Cost-Effective Perovskite

- Solar Cells, *Adv. Funct. Mater.* 31 (2021). <https://doi.org/10.1002/adfm.202006803>.
- [9] T. Wu, P. Xu, D. Wang, X. Jiang, F. Guo, S. Gao, Z. Ge, Y. Zhang, One-step synthesis of low-cost perylenediimide-based cathode interfacial materials for efficient inverted perovskite solar cells, *Chem. Eng. J.* 454 (2023) 140451. <https://doi.org/10.1016/j.cej.2022.140451>.
- [10] R. Sharma, A. Sharma, S. Agarwal, M.S. Dhaka, Stability and efficiency issues, solutions and advancements in perovskite solar cells: A review, *Sol. Energy.* 244 (2022) 516–535. <https://doi.org/10.1016/j.solener.2022.08.001>.
- [11] D. Lan, M.A. Green, Combatting temperature and reverse-bias challenges facing perovskite solar cells, *Joule.* 6 (2022) 1782–1797. <https://doi.org/10.1016/j.joule.2022.06.014>.
- [12] N.A.N. Ouedraogo, H. Yan, C.B. Han, Y. Zhang, Influence of Fluorinated Components on Perovskite Solar Cells Performance and Stability, *Small.* 17 (2021). <https://doi.org/10.1002/sml.202004081>.
- [13] W. Xiang, S. (Frank) Liu, W. Tress, Interfaces and Interfacial Layers in Inorganic Perovskite Solar Cells, *Angew. Chemie.* 133 (2021) 26644–26657. <https://doi.org/10.1002/ange.202108800>.
- [14] S. Yang, Y. Duan, Z. Liu, S. Liu, Recent Advances in CsPbX₃ Perovskite Solar Cells: Focus on Crystallization Characteristics and Controlling Strategies, *Adv. Energy Mater.* 2201733 (2022) 1–28. <https://doi.org/10.1002/aenm.202201733>.
- [15] Z. Guo, L. Gao, Z. Xu, S. Teo, C. Zhang, Y. Kamata, S. Hayase, T. Ma, High Electrical Conductivity 2D MXene Serves as Additive of Perovskite for Efficient Solar Cells, *Small.* 14 (2018) 1–8. <https://doi.org/10.1002/sml.201802738>.
- [16] L. Yang, Y. Dall’Agnese, K. Hantanasirisakul, C.E. Shuck, K. Maleski, M. Alhabeab, G. Chen, Y. Gao, Y. Sanehira, A.K. Jena, L. Shen, C. Dall’Agnese, X.F. Wang, Y. Gogotsi, T. Miyasaka, SnO₂-Ti₃C₂ MXene electron transport layers for perovskite solar cells, *J. Mater. Chem. A.* 7 (2019) 5635–5642. <https://doi.org/10.1039/c8ta12140k>.
- [17] Y. Niu, C. Tian, J. Gao, F. Fan, Y. Zhang, Y. Mi, X. Ouyang, L. Li, J. Li, S. Chen, Y. Liu,

- H.L. Lu, X. Zhao, L. Yang, H. Ju, Y. Yang, C.F. Ding, M. Xu, Q. Xu, Nb₂C MXenes modified SnO₂ as high quality electron transfer layer for efficient and stability perovskite solar cells, *Nano Energy*. 89 (2021) 106455.
<https://doi.org/10.1016/j.nanoen.2021.106455>.
- [18] I. Ali, M. Faraz Ud Din, Z.G. Gu, MXenes Thin Films: From Fabrication to Their Applications, *Molecules*. 27 (2022) 1–38. <https://doi.org/10.3390/molecules27154925>.
- [19] S.A.A. Shah, M.H. Sayyad, K. Khan, J. Sun, Z. Guo, Application of mxenes in perovskite solar cells: A short review, *Nanomaterials*. 11 (2021) 1–17.
<https://doi.org/10.3390/nano11082151>.
- [20] Y. Gogotsi, B. Anasori, The Rise of MXenes, *ACS Nano*. 13 (2019) 8491–8494.
<https://doi.org/10.1021/acsnano.9b06394>.
- [21] A.D. Dillon, M.J. Ghidui, A.L. Krick, J. Griggs, S.J. May, Y. Gogotsi, M.W. Barsoum, A.T. Fafarman, Highly Conductive Optical Quality Solution-Processed Films of 2D Titanium Carbide, *Adv. Funct. Mater.* 26 (2016) 4162–4168.
<https://doi.org/10.1002/adfm.201600357>.
- [22] V. Nádaždy, F. Schauer, K. Gmucová, Energy resolved electrochemical impedance spectroscopy for electronic structure mapping in organic semiconductors, *Appl. Phys. Lett.* 105 (2014). <https://doi.org/10.1063/1.4898068>.
- [23] F. Schauer, V. Nádaždy, K. Gmucová, Electrochemical impedance spectroscopy for study of electronic structure in disordered organic semiconductors - Possibilities and limitations, *J. Appl. Phys.* 123 (2018) 161590. <https://doi.org/10.1063/1.5008830>.
- [24] H. Bäessler, D. Kroh, F. Schauer, V. Nádaždy, A. Köhler, Mapping the Density of States Distribution of Organic Semiconductors by Employing Energy Resolved–Electrochemical Impedance Spectroscopy, *Adv. Funct. Mater.* 31 (2021).
<https://doi.org/10.1002/adfm.202007738>.